Since January 2020 Elsevier has created a COVID-19 resource centre with free information in English and Mandarin on the novel coronavirus COVID-19. The COVID-19 resource centre is hosted on Elsevier Connect, the company's public news and information website.

Elsevier hereby grants permission to make all its COVID-19-related research that is available on the COVID-19 resource centre - including this research content - immediately available in PubMed Central and other publicly funded repositories, such as the WHO COVID database with rights for unrestricted research re-use and analyses in any form or by any means with acknowledgement of the original source. These permissions are granted for free by Elsevier for as long as the COVID-19 resource centre remains active.

VIROLOGY 198, 405–411 (1994)

Distinct Structural Elements and Internal Entry of Ribosomes in mRNA3 Encoded by Infectious Bronchitis Virus

SHU-YUN LE,[1] NAHUM SONENBERG,* AND JACOB V. MAIZEL, JR.

*Laboratory of Mathematical Biology, Division of Cancer Biology, Diagnosis and Centers, National Cancer Institute, NIH, Building 469, Room 151, Frederick, Maryland 21702; and *Department of Biochemistry and McGill Cancer Center, McGill University, Montreal, Quebec, Canada H3G 1Y6*

Received August 30, 1993; accepted October 7, 1993

Infectious bronchitis virus (IBV) mRNA3 encodes three small proteins, 3a, 3b, and 3c, at its 5′ end. Recently, it was demonstrated that initiation of protein 3c is dependent on the upstream sequence. Monte Carlo simulations of RNA folding in this tricistronic mRNA3 indicate that a highly significant folding region occurs prior to the initiator AUG of 3c. The unusual folding region (UFR) of 265 nucleotides (nt) contains the coding sequences of proteins 3a and 3b. Details of the structural analyses show that five highly significant RNA stem–loops in the UFR can be modeled into a compact superstructure by the interaction of two predicted pseudoknot structures. The folded superstructure comprising nt 44 to 330, with additional 22 nt downstream from this UFR, is suggested to serve as a ribosome landing pad (or an internal ribosomal entry site) in the cap-independent translation of the 3c of IBV. Intriguingly, the proposed structural motif of this coronavirus shares structural features similar to those proposed in a number of picornavirus mRNAs. Based on the common structural features, a plausible base pairing model between mRNA3 and 18 S rRNA is suggested, which is consistent with a general mechanism for regulation of internal initiation described in many picornaviruses. © 1994 Academic Press, Inc.

The mRNA3 of the coronavirus infectious bronchitis virus (IBV) has been demonstrated to be functionally tricistronic (*1*). The three small proteins, 3a, 3b, and 3c, encoded at the 5′ end of the mRNA3 are expressed in infected cells. Although the exact mechanism of translational initiation of this tricistronic mRNA is unclear, recent experiments (*2*) suggest that the translation of 3c utilizes a mechanism which differs from the ribosomal scanning process employed in the translational initiation of most eukaryotic mRNAs (*3, 4*). Mutagenesis studies (*2*) indicated that the 3c initiation depends on the upstream sequence that might function as a ribosome landing pad (RLP); however, the precise RLP in IBV is still undetermined. Also, the precise mechanism for the internal entry and binding of ribosomes, as well as the translational initiation in mRNA3, remains unclear.

Recently, we have proposed a common higher-order RNA structural model for the RLPs of all picornaviruses that consists of conserved RNA secondary and tertiary structural elements (*5, 6*). The higher-order RNA structural conformation in the common superstructure was proposed to be specifically recognized by components of the translational apparatus, 40 S ribosomal subunit, and/or *trans*-acting factor(s) to promote cap-independent translation of picornaviruses. The structural role of the RLP is considered to be crucial for the ribosome binding directly at mRNAs in the initiation of translation. According to the suggested common structural motif, a conserved base pairing model between picornaviruses and 18 S rRNA can provide a rational interpretation for currently available mutagenesis data from the 5′ nontranslated region (5′NTR) of picornaviruses.

To find putative RLPs and better understand the mechanism of internal initiation of cap-independent translation in the mRNA3 of IBV, unusual folding regions (UFRs) are searched in sliding windows (*7–9*) throughout the mRNA3 sequence of IBV. This is based on the calculations of significance score (Sigscr) and stability score (Stbscr) that are used to evaluate RNA folding occurring in the test sequence. Plausible structural motifs in the predicted UFR upstream of the 3c open reading frame (ORF) are proposed in this report. Furthermore, the base pairing model between IBV mRNA3 and 18 S rRNA suggested in this study shares a structural feature similar to that formed between 18 S rRNA and RLP of picornaviruses. The common feature is that the complementary sequence to 18 S rRNA occurs 3′ from a distinct pseudoknot structure and is several nucleotides (nt) prior to the initiator AUG of ORF (however, this differs from rhinoviruses in which the site is about 180 nt prior to the initiator AUG). Also, the complementary sequence at the 3′-end of 18 S rRNA with both IBV and picornaviruses is conserved for its sequence position. This indicates that the common structural features in these diverse RNAs from picornavirus to IBV may function in the mediation of internal initiation of cap-independent translation.

[1] To whom reprint requests should be addressed.

0042-6822/94 $5.00
Copyright © 1994 by Academic Press, Inc.
All rights of reproduction in any form reserved.

In this study, five mRNA3 sequences encoding 3a, 3b, and 3c were used. The sequence data were derived from GenBank database (Release 72.0, June 15, 1992) and their loci in GenBank are IBBIBV3A (strain Portugal/322/82), IBV3ABC (strain UK/68/84), IBBIBV3B (strain UK/183/66), and IBV3RNABC (strain M41). The sequence data for Beaudette strain were from Ref. 1. In the computer simulation the mRNA3 sequence (strain Portugal/322/82) was referred to as ibv3a and used throughout the study.

Based on the large number of experimental data (*36, 43–46*), we have known that some RNA functional elements closely correlate with local RNA foldings in the viral RNAs. In recent years a number of results from computer simulations associated with extensive mutagenesis studies (*10–12, 47*) have demonstrated that the distinct UFRs identified in retroviral mRNAs detected by our procedures (*8, 9*) correlate with various activities in transcription and translation. An UFR in an RNA sequence, here, is regarded as a region that is both statistically more significant (lower Sigscr) and highly stable (lower Stbscr) relative to other possible foldings found in the sequence. Thus, it is assumed to have a significant folding pattern implying a structural role for the sequence information. UFRs in mRNA3 were detected by an extensive Monte Carlo simulation, SEGFOLD (*8, 9*). In the simulation, window size changed from 40 to 300 nt with 2-nt increments for ibv3a and strain UK/183/66 and from 25 to 299 nt for the other two strains. For each window, statistical significance (measured by Sigscr) of an RNA folding was evaluated by comparing the predicted lowest free energy of the actual segment in the sequence with those of its random permutations in sliding a window throughout the sequence. Similarly, thermodynamically relative stability (measured by Stbscr) of RNA folding was assessed by comparing the stability of the actual segment with those of other possible foldings in the sequence. Simulations of the lowest free energy were calculated using the Turner (*13, 14*) or Tinoco (*15, 16*) energy rule. The results reveal that the largest optimized window is 264 nt (45–308) in the simulation. Further analysis using a 265-nt window shows that the largest identified UFR W in ibv3a can be adjusted to be a 265-nt segment from nt 44 to 308 (see Fig. 1a). This UFR W comprises five local UFRs, A–E. The UFR A contains nt 44 to 121, B 140 to 172, C 195 to 236, D 248 to 269, and E 277 to 308. Three local UFRs, A–C, are delineated in Figs. 1b–1c.

Using the same procedure and parameters as above, the largest UFRs identified in mRNA3 sequences of strains UK/183/66, UK/68/84, and M41 are the segments 46–313, 45–309, and 44–308, respectively. A continued statistical analysis for the distributions of significant scores and stability scores was performed by averaging the Sigscr and Stbscr in each sequence position for four strains of IBV (see Fig. 2). It is clear that a distinct, highly significant and stable RNA folding region (265 nt) consistently occurs 44, 45, or 46 nt downstream from the initiator AUG of the 3a ORF. It should be mentioned that the sequence from strain Beaudette, which is almost identical with that of M41, is not included in the statistical analysis to avoid excessive bias from overrepresented sequence. Thus, the largest UFR W identified in ibv3a is a common feature for all IBV sequences.

The possible RNA secondary structures in the predicted UFR W (44–308) of ibv3a were predicted by EFFOLD (*17*), an improved method for predicting alternative RNA secondary structures. The uncertainties of energy parameters for RNA folding were considered in the prediction. In the computer simulation, the free energy parameters from the Turner energy rule (*13*) were perturbed about their tabular values based on a normal distribution within the ranges of their experimental errors (*13, 18*). The lowest free energy structure was searched for each "simulated energy rule." Fifty energy rules and their corresponding structures with lowest free energies were generated in the computational experiment. These computed structures were then compared to each other and the frequency of each distinct stem predicted in the simulation was calculated. As a result, 34 different stems were compiled. Among them, five stem–loop structures (labeled by letters A–E; see Figs. 3 and 4) were most favored in the simulation. The recurring ratios for the stem–loops B, C, and E are 100% and ratios of helical stems in stem–loops A and D are at least 94%. The frequently recurring feature of these predicted stems in RNA folding simulations was also observed in other strains. The validity of predicted helices was then examined further by their conservation in five homologous sequences (see Fig. 3). Sequence comparison indicated that the five stem–loop structures were conserved in five se-

FIG. 1. Distributions of significance and stability scores in IBV mRNA3 sequence. The profile was obtained by plotting the significance scores (continuous lines) and stability scores (broken lines) against the position of the middle nt in the window by sliding the window throughout the sequence. The significance score $((E - E_r)/SD_r)$ and stability score $((E - E_w)/SD_w)$ computed by using the Turner (*13, 14*) and Tinoco energy rules (*15, 16*) are represented by thick and thin lines, respectively, where E is the lowest free energy of formation for RNA folding of a specific RNA fragment, letting E_r and SD_r, respectively, be the mean and standard deviation of E for a random shuffling of RNA foldings and letting E_w and SD_w be the mean and standard deviation of E resulting from sliding a window. The horizontal line represents the value of 3.1 standard scores. The identified UFR W, A, B, and C are marked and labeled. (a) Profile for window length of 265 nt. The positions for the start segment (1–265) and the last segment (366–630) are numbered 133 (265/2 + 1) and 498 in the map, respectively. (b) Window size is 78 nt (position for segment 1–78 is 39) and (c) window size is 42 nt (start position is 21).

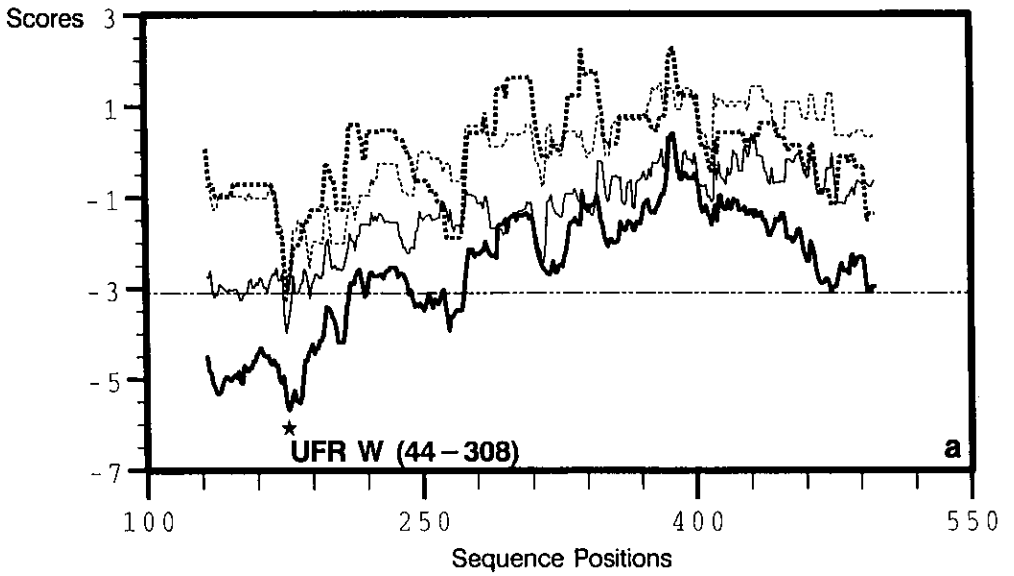
Scores
3
1
-1
-3
-5
-7
UFR W (44–308)
a
100
250
400
550
Sequence Positions

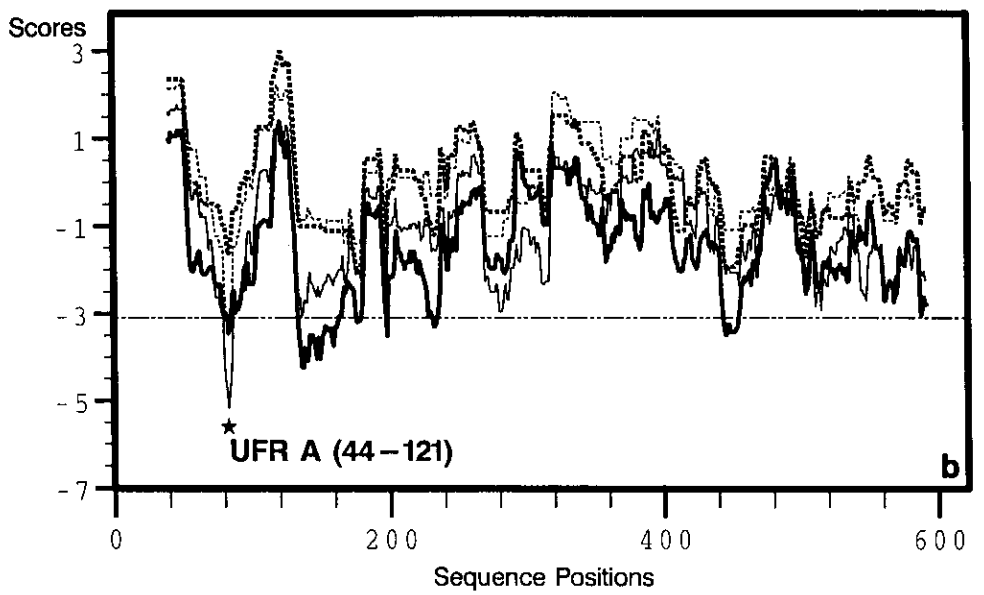
Scores
3
1
-1
-3
-5
-7
UFR A (44–121)
b
0
200
400
600
Sequence Positions

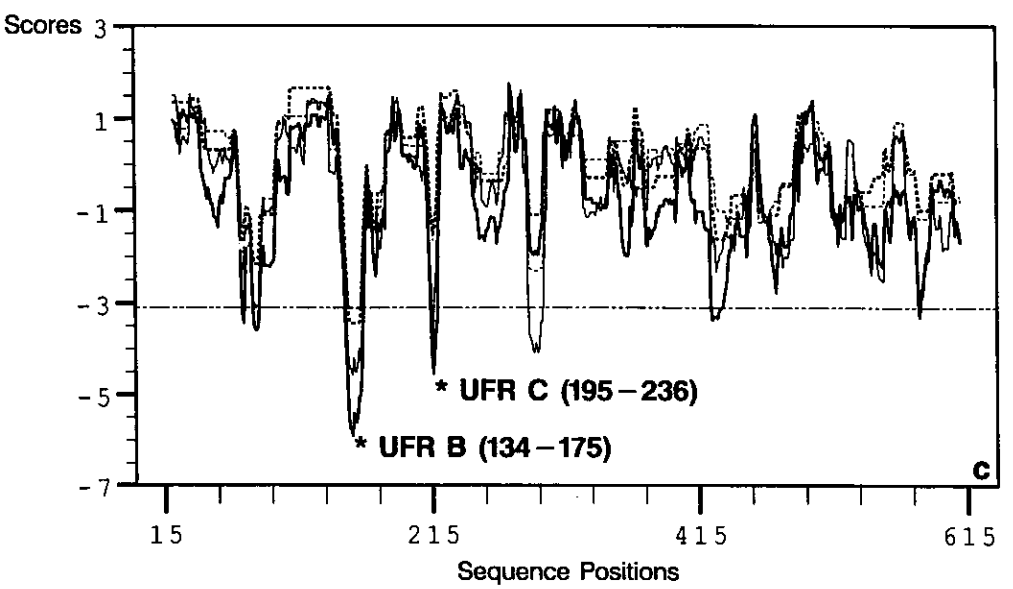
Scores
3
1
-1
-3
-5
-7
* UFR C (195–236)
* UFR B (134–175)
c
15
215
415
615
Sequence Positions

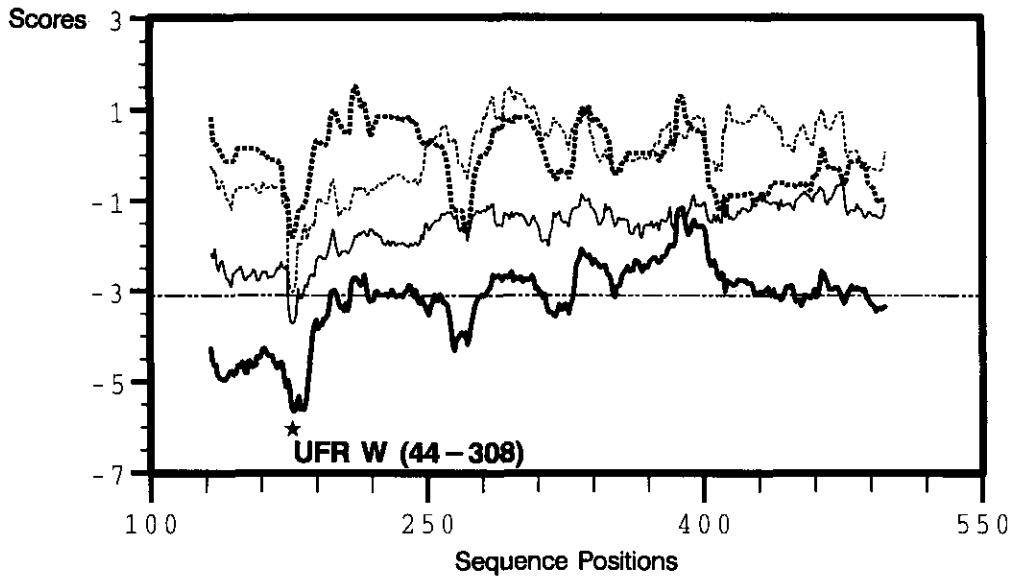

FIG. 2. Combined profile of the distributions for the significance and stability scores in four IBV mRNA3 sequences (strains M41, UK/68/84, UK/183/66, and Portugal/322/82). In the profile the significance score (continuous line) and stability score (broken line) were made by averaging their scores in each position based on their alignment (see Fig. 3). The window size is 265 nt. For further details see the legend to Fig. 1.

quences. Interestingly, these five thermodynamically favored stem–loops precisely correspond to those five UFRs A–E identified in SEGFOLD, respectively (see Fig. 1). The structural feature of high stability and the unusual statistical significance of these stem–loops are consistent with those identified in RLP of all picornaviruses (*5, 6, 42*).

Based on these predicted five stem–loop structures, possible tertiary interactions within UFR W and its neighborhood were searched using RNAKNOT (*19*). Three pseudoknots were found in the simulation and one of them is not highly conserved among five sequences. This pseudoknot is not included in the common structural model. The proposed pseudoknot K1 connects stem–loops B and C, and K2 links the UFR W with its downstream segment prior to the initiator. Thus, these tertiary interactions contribute to the formation of a compact folded superstructure (see Fig. 3) in the upstream sequence element from the initiator AUG of the 3c ORF. This superstructure model is different from the published model (*2*) based on folding the total 5′NTR by an older program. Between two tertiary structural elements, the predicted pseudoknot K1 shows unusual statistical significance and high thermodynamic stability relative to randomly shuffled sequences. This distinctive tertiary structural element is supported by compensatory base changes observed in the five mRNA3 sequences (Fig. 3). This predicted pseudoknot becomes entangled with the base pairing between region 183–187 and region 209–213 within the 3b-encoded sequence of ibv3a. In the proposed model, the computed tertiary structural element K2 that includes 22 nt downstream from the identified UFR is intermediately stable and statistically significant above the random background. Although K2 is conserved in the five mRNA3 sequences, no evidence of compensatory base changes was observed.

In the computed structure, base pairing between IBV mRNA3 and 18S rRNA is proposed (see Fig. 4). In our model, 8 nt in the single-stranded region (1823 to 1837) at the 3′ end of 18 S rRNA that is followed by a significantly stable stem–loop structure (*20*) are complementary to the single-stranded region upstream of the initiator AUG of the 3c ORF. The complementary sequence to 18 S rRNA follows the pseudoknot K2. This feature is analogous to that found in the base pairing model between picornaviral RNA and 18 S rRNA (*5, 6*). The sequences complementary to mRNA3 and picornaviruses presented here are not only conserved evolutionally among all 18 S rRNAs of eukaryotes (*21*) but also conserved in their positions in the sequence. Chemical and RNase probing results also indicate that these two complementary sequences are not involved in the base pairing interaction of the published RNA secondary structural model of 18 S rRNAs (*22*). We suggest that these complementary sequences to the 18 S rRNA in the supposed RLP of IBV, similar to those in RLP of picornaviruses (*5, 6, 32*), play an important role in a manner analogous to that of the Shine–Dalgarno sequence documented for the translational initiation of prokaryotic mRNAs (*23*).

A recent mutagenesis study (*2*) has suggested that a nucleotide sequence within the 3b ORF and at least a portion of the 3a ORF are important for cap-independent initiation of the 3c ORF. The theoretical higher-order structure proposed in the UFR W and its downstream sequence upstream of the initiator of the 3c are conserved in five mRNA3 sequences. The predicted

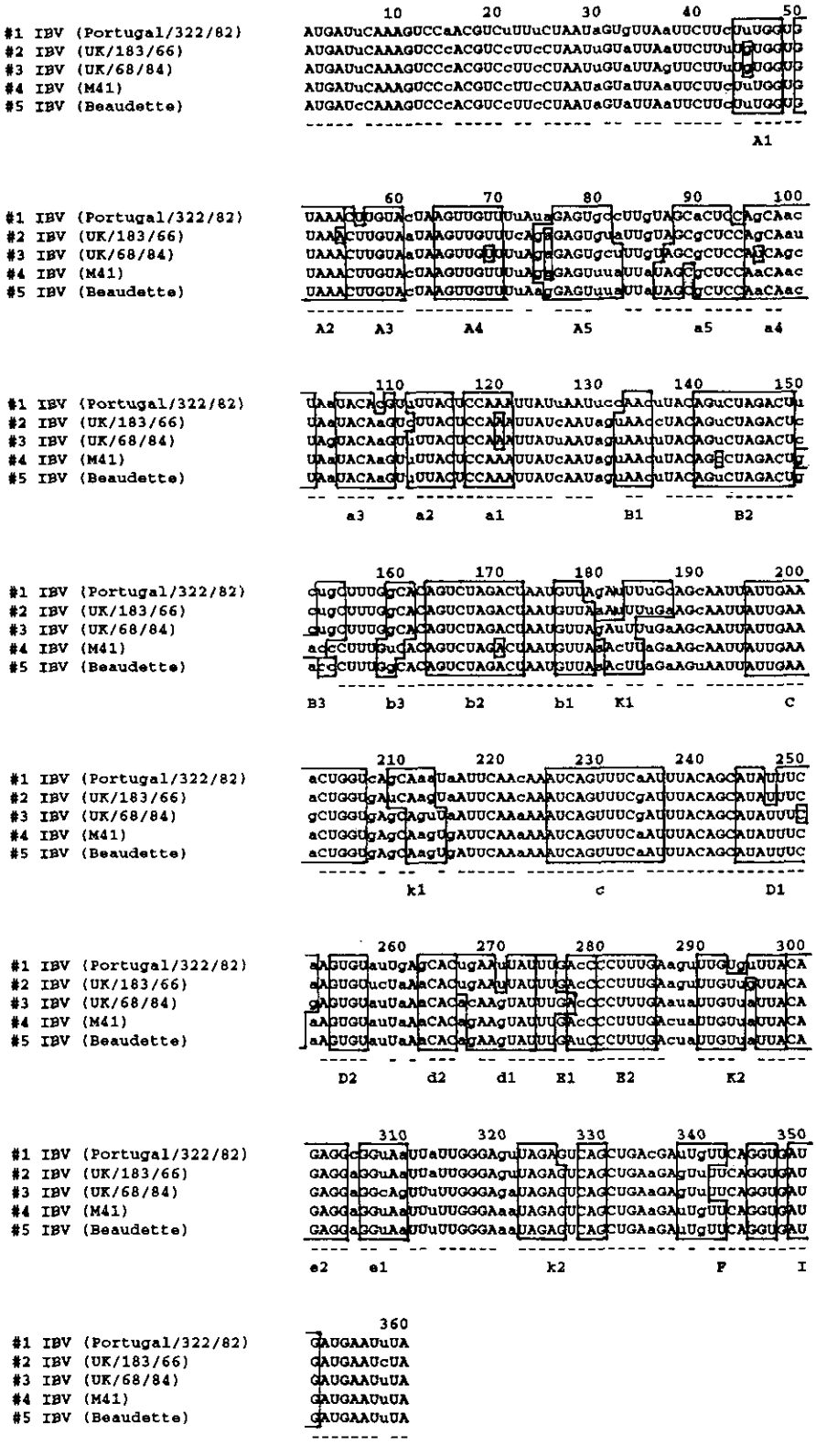

FIG. 3. Alignment of UFRs in the 5′ NTRs of coronavirus infectious bronchitis virus (IBV) mRNA3 from strains Portugal/322/82, UK/183/66, UK/68/84, M41, and strain Beaudette. Conserved nucleotides are denoted by dashes. The conserved base pairings are marked by boxes. Among them, boxes A1–A5 and a1–a5 denote the significant stem–loop structure A, B1–B3 and b1–b3 for stem–loop B, C and c for stem–loop C, D1–D2 and d1–d2 for stem–loop D, E1–E2 and e1–e2 for stem loop E, and K1–K2 and k1–k2 denote the two predicted pseudoknots K1 and K2. The box F shows the complementary sequence with 18 S rRNA and box I shows the initiator of the c3 protein.

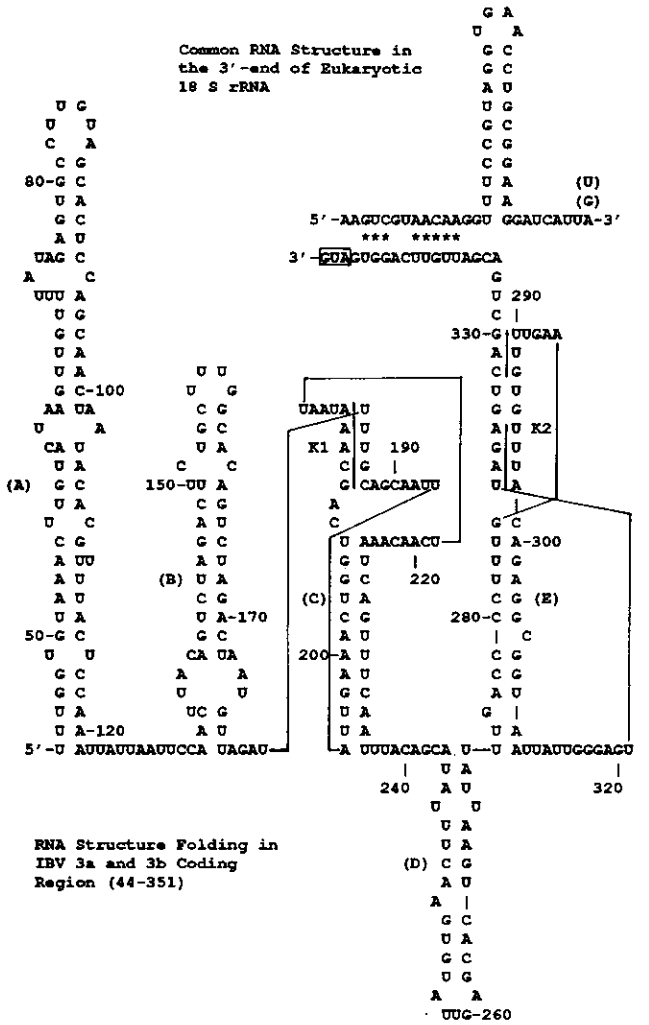

FIG. 4. Predicted base pairing model between the proposed RLP of IBV mRNA3 (strain Portugal/322/82) and 18 S rRNA. The tertiary interactions in the model are denoted by letters K1–K2 and five highly significant and stable RNA stem–loops are indicated by (A)–(E), respectively. The RNA secondary structure of 18 S rRNA is based on the published model (*7, 12, 37*). An asterisk between two sequences denotes the base pairing between viral RNAs and human 18 S rRNA. The initiator AUG of the 3c is boxed.

structure shows high stability and statistical significance based on the randomized permutations of RNA folding. Our results strongly suggest that this predicted superstructure, folded from nt 44 to 330 (an UFR plus additional 22 nt downstream fragment), can serve as a RLP of the mRNA3 in a manner similar to that delineated for picornaviruses. The significant folding form in the RLP of mRNA3 is suggested to play a crucial structural role for its sequence information. Although this assumed RLP in IBV lacks the polypyrimidine tract that is present in the picornavirus 5′NTR and it is located at the ORFs of 3a and 3b, rather than within the untranslated region, the similarity of the structural features between the base pairing models of mRNA3–18 S rRNA and picornavirus 18 S rRNA is visible. This consistent structural feature from picornavirus to IBV implies that the RNA higher-order structure proposed in this paper has a general function in the internal initiation of cap-independent translation.

Several lines of evidence indicate that the 5′NTR of picornaviruses promotes cap-independent translation initiation in which the ribosome is directed to bind with RLP without scanning from the 5′ terminus of 5′NTR (*24–33*). The RNA tertiary structure folded in RLP of picornaviruses is proposed to play an indispensable role in the regulation of internal translation (*5, 6*). Although the proposed tertiary structure in this study needs to be verified by experiments, a similar model proposed for picornaviruses can provide a reasonable explanation for available mutagenesis data (*30, 32, 34, 35*) in the translational initiation of these viral RNAs.

Mutagenesis studies from a number of laboratories have also indicated that pseudoknot structures can function as recognition sites for protein binding to mRNAs (*36–39*). If the distinct configuration of a pseudoknot is destroyed, its biological function will be reduced or abolished. We have proposed that the process of ribosomal binding to the RLP of picornaviruses (*5, 6*) may involve the recognition of specific RNA structures within RLP by particular proteins, such as the 40 S ribosomal subunit or p52 protein (*40*). Several efficient binding sites in RLP of picornaviruses by cellular proteins have also been reported (*40, 41*). Taken together, the proposed pseudoknot structures, K1 and K2, formed in the superstructure of IBV are assumed to function as efficient binding sites for ribosome and/or other initiation factors in the translational initiation. This is analogous to that suggested for the conserved pseudoknots of picornaviruses (*5, 6*). In addition, a twofold symmetry of five base pairs exists within the stem–loop B (AGUCUAGACU and AGUCUAGACU). This dyad structural element can be assumed to provide a recognition site for a dimeric RNA binding protein. We suggest that it is the structural role of RLP for IBV that is crucial in its internal initiation of cap-independent translation.

REFERENCES

1. LIU, D. X., CAVANAGH, D., GREEN, I. J., and INGLIS, S. C., *Virology* **184,** 531–544 (1991).
2. LIU, D. X., and INGLIS, S. C., *J. Virol.* **66,** 6143–6154 (1992).
3. KOZAK, M., *J. Cell Biol.* **108,** 229–241 (1989).
4. KOZAK, M., *J. Cell Biol.* **115,** 887–903 (1991).
5. LE, S.-Y., CHEN, J.-H., SONENBERG, N., and MAIZEL, J. V., JR., *Virology* **191,** 858–866 (1992).
6. LE, S.-Y., CHEN, J.-H., SONENBERG, N., and MAIZEL, J. V., JR., *Nucleic Acids Res.* **21,** 2445–2451 (1993).
7. LE, S.-Y., CHEN, J.-H., BRAUN, M. J., GONDA, M. A., and MAIZEL, J. V., JR., *Nucleic Acids Res.* **16,** 5153–5268 (1988).
8. LE, S.-Y., CHEN, J.-H., and MAIZEL, J. V., JR., *In* "Structure & Methods: Human Genome Initiative and DNA Recombina-

tion" (R. H. Sarma and M. H. Sarma, Eds.), Vol. 1, pp. 127–136. Adenine Press, Albany, NY, 1990.
9. Le, S.-Y., Malim, M. H., Cullen, B. R., and Maizel, J. V., Jr., *Nucleic Acids Res.* **18,** 1613–1623 (1990).
10. Malim, M., Hauber, J., Le, S.-Y., Maizel, J. V., Jr., and Cullen, B. R., *Nature* **338,** 254–257 (1989).
11. Fenrick, R., Malim, M., Hauber, J., Le, S.-Y., Maizel, J. V., Jr., and Cullen, B. R., *J. Virol.* **63,** 5006–5012 (1989).
12. Tiley, L. S., Brown, P. H., Le, S.-Y., Maizel, J. V., Jr., Clements, J. E., and Cullen, B. R., *Proc. Natl. Acad. Sci. USA* **87,** 7497–7501 (1990).
13. Freier, S. M., Kierzek, R., Jaeger, J. A., Sugimoto, N., Caruthers, M. H., Neilson, T., and Turner, D. H., *Proc. Natl. Acad. Sci. USA* **83,** 9373–9377 (1986).
14. Jaeger, J. A., Turner, D. H., and Zuker, M., *Proc. Natl. Sci. USA* **86,** 7706–7710 (1990).
15. Salser, W., *Cold Spring Harbor Symp. Quant. Biol.* **42,** 985–1002 (1977).
16. Cech, T. R., Tanner, N. K., Tinoco, I., Jr., Weir, B. R., Zuker, M., and Perlman, P. S., *Proc. Natl. Acad. Sci. USA* **80,** 3903–3907 (1983).
17. Le, S.-Y., Chen, J.-H., and Maizel, J. V., Jr., *Nucleic Acids Res.* **21,** 2173–2178 (1993).
18. Williams, A. L., and Tinoco, I., Jr., *Nucleic Acids Res.* **14,** 299–315 (1993).
19. Chen, J.-H., Le, S.-Y., and Maizel, J. V., Jr., *Comp. Appl. Biosci.* **8,** 243–248 (1992).
20. Le, S.-Y., and Maizel, J. V., Jr., *J. Theor. Biol.* **138,** 495–510 (1989).
21. Huysmans, E., and Wachter, R., *Nucleic Acids Res.* **14,** r73–r118 (1986).
22. Rairkar, A., Rubino, H. M., and Lockard, R. E., *Biochemistry* **27,** 582–592 (1988).
23. Shine, J., and Dalgarno, L., *Proc. Natl. Acad. Sci. USA* **71,** 1342–1346 (1974).
24. Trono, D., Andino, R., and Baltimore, D., *J. Virol.* **62,** 2291–2299 (1988).
25. Pelletier, J., and Sonenberg, N., *Nature* **334,** 320–325 (1988).
26. Bienkowska-Szewczyk, K., and Ehrenfeld, E., *J. Virol.* **62,** 3068–3072 (1988).
27. Brown, E. A., Day, S. P., Jansen, R. W., and Lemon, S. M., *J. Virol.* **65,** 5828–5838 (1991).
28. Duke, G. M., Hoffman, M. A., and Palmenberg, A. C., *J. Virol.* **66,** 1602–1609 (1992).
29. Borman, A., and Jackson, R. J., *Virology* **188,** 685–696 (1992).
30. Kuhn, R., Luz, N., and Beck, E., *J. Virol.* **64,** 4625–4631 (1990).
31. Jang, S. K., Davies, M. V., Kaufman, R. J., and Wimmer, E., *J. Virol.* **63,** 1651–1660 (1989).
32. Pilipenko, E. V., Gmyl, A. P., Maslova, S. V., Svitkin, Y. V., Sinyakov, A. N., and Agol, V. I., *Cell* **68,** 119–131 (1992).
33. Randyopadhyay, P. K., Wang, C., and Lipton, H. L., *J. Virol.* **66,** 6249–6256 (1992).
34. Nicholson, R., Pelletier, J., Le, S.-Y., and Sonenberg, N., *J. Virol.* **65,** 5886–5894 (1991).
35. Pestova, T. V., Hellen, C. U. T., and Wimmer, E., *J. Virol.* **65,** 6194–6204 (1991).
36. Brierley, I., Digard, P., and Inglis, S. C., *Cell* **57,** 537–547 (1989).
37. Brierley, I., Rolley, N. J., Jenner, A. J., and Inglis, S. C., *J. Mol. Biol.* **220,** 889–902 (1991).
38. Tang, C. K., and Draper, D. E., *Cell* **57,** 531–536 (1989).
39. McPheeters, D. S., Stormo, G. D., and Gold, L., *J. Mol. Biol.* **201,** 517–535 (1988).
40. Meerovitch, K., Svitkin, Y. V., Lee, H. S., Lejbkowicz, F., Kenan, D. J., Chan, E. K. L., Agol, V. I., Keene, J. D., and Sonenberg, N., *J. Virol.* **67,** 3798–3807 (1993).
41. Scheper, G. C., Thomas, A., and Voorma, H. O., *Biochim. Biophys. Acta* **1089,** 220–226 (1991).
42. Le, S.-Y., and Zuker, M., *J. Mol. Biol.* **216,** 729–741 (1990).
43. Feng, S., and Holland, E. C., *Nature* **334,** 165–167 (1988).
44. Muesing, M. A., Smith, D., and Capon, D., *Cell* **48,** 691–701 (1987).
45. Esteban, R., Fujimura, T., and Wickner, R. B., *EMBO J.* **8,** 947–954 (1989).
46. Jacks, T., Power, M. D., Masiarz, F. R., Luciw, P. A., Barr, P. J., and Varmus, H. E., *Nature* **331,** 280–283 (1988); Jacks, T., Madhani, H. D., Masiarz, F. R., and Varmus, H. E., *Cell* **55,** 447–458 (1988).
47. Hanly, S. M., Rimsky, L. T., Malim, M. H., Kim, J. H., Hauber, J., Duc Dodon, M., Le, S.-Y., Maziel, J. V., Cullen, B. R., and Greene, W. C., *Genes Dev.* **3,** 1534–1544 (1989).